www.rericjournal.ait.ac.th

Experimental and Numerical Assessment of the Influence of Heat Trap Assembly on Solar Chimney Performance

Iylia E. Abdul Jamil*, [1], Hussain H. Al-Kayiem[+], and Syed I.U. Gilani*

ARTICLE INFO

Article history:
Received 26 September 2023
Received in revised form
29 January 2024
Accepted 15 March 2024

Keywords:
Heat trap assembly
Solar chimney performance
Solar collector
Solar thermal absorption
Solar updraft tower

ABSTRACT

A big hurdle to using solar chimneys for power generation is their low overall efficiency, which is measured by how effectively energy is converted at different stages of the system. While a taller chimney might help, it is expensive and complex to implement. To address this issue, a new study explored the possibility of using a thermal absorbing assembly at the top of the chimney to increase its efficiency without increasing its height. The study presented both experimental and numerical data on this approach, looking at changes in temperature and heat gains as performance indicators. By adding this low-cost and simple fixture, the study found that the temperature before the chimney outlet increased, and the stack effect was strengthened. The rise of air temperature posed an increase of up to 83.1% by experimental assessment and an increase of 12.75% by numerical assessment with the added fixture of the heat trap.

1. INTRODUCTION

The solar chimney power plant (SCPP) is a solar updraft technology for electricity generation that utilizes the heat from solar energy. It has three major components: a solar collector, a chimney tower, and a wind turbine. The SCPP's straightforward working principle is appealing; solar radiation penetrates the collector roof which transfers thermal energy to the air underneath it. This energy transfer is further enhanced by the greenhouse effect created under the semi-transparent material of the collector roof [1]. The hot air then moves toward the chimney base, which results in a continuous updraft as hot air is guided toward the chimney exit. At the same time, ambient air continuously enters the system from the peripheral inlet of the solar collector at the ground. The wind turbine, situated at the base of the chimney, utilizes the kinetic energy from the air that runs through it [2].

The air mass flow rate in the SCPP is influenced by the increase in air temperature under the collector and the solar chimney height. The chimney efficiency is low compared to the other components of the SCPP [3], [4], which brings down the plant's overall efficiency. The power output from the SCPP highly depends on the system's overall scale [5], [6] and the chimney height is key to its efficiency [7], [8]. In attaining the maximum generated power by the SCPP, a limit was imposed on the maximum collector size, while modern technology permits the construction of comparably larger-scaled chimneys [9], [10].

For a long period, the size of the system, which includes the chimney height, has been the determining factor in the system's ability to produce [11]. More recently, optimization works have been done to find novel unconventional designs for the chimney tower. Different chimney configurations have been explored by researchers, which include divergent chimneys and sloped chimney inlets with varying plant scales [4], [12], [13]. Other than chimney geometry, the floating solar chimney has been explored to investigate its performance when exposed to external crosswinds [14]. Findings on air temperature distribution inside the chimney are limited in SCPP applications, while focus has been given to enhancing the collector roof design and the storage of thermal energy in the ground [13], [15], [16].

One of the methods to increase the SCPP efficiency is increasing the updraft velocity in the chimney. This is achievable when there is a higher difference in air temperature between the ambient and the top exit of the solar chimney body. As the air temperature at the chimney exit increases, the density of air in that region will decrease at the same time, which results in a greater difference in air density and pressure between the bottom and top of the chimney, thus improving the flow.

This article explores this theory by adding a heat trap, which is a thermal absorption fixture, at the top of the chimney, as shown in Figure 1. The heat trap theoretically can absorb solar radiation, enhance heat transfer to the air at the chimney exit, and create a bigger pressure difference that would drive the airflow through the system.

Experimental and numerical results are presented in this article to suggest the possibility of improving

*Mechanical Engineering Department, Universiti Teknologi PETRONAS, 32610 Seri Iskandar, Perak, Malaysia.

[+]Hilla University College, 51001 Ranjia, Babylon, Iraq.

[1]Corresponding author:
Email: iylia_0008404@utp.edu.my

chimney performance with the heat trap assembly, including comparisons made with a conventional chimney performance of the same height. The following subsections begin with the design theory behind the SCPP, followed by the developed model description for both the experimental and numerical investigations. This includes specifications of the typical solar chimney components and the proposed heat trap. Next, measurement data are presented to compare the different cases tested. Finally, the performance of the different cases is calculated in terms of the temperature rise and air velocity.

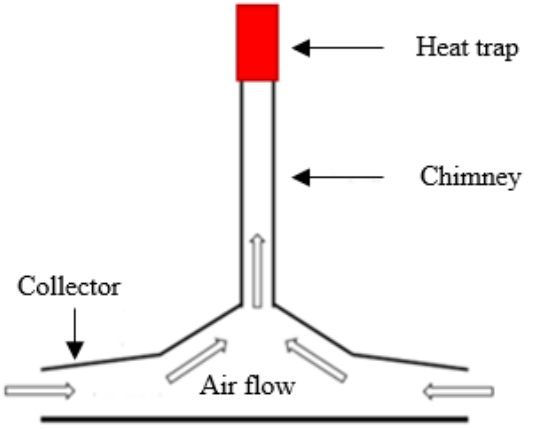

Fig. 1. The SCPP schematic diagram, with novel heat trap assembly.

2. GOVERNING EQUATIONS

The theory of the SCPP is described in this section, for parts of the system components. Governing equations are applied in numerical simulation to calculate the results.

2.1 The Solar Collector

The solar collector component is responsible for converting solar radiation to thermal energy. It comprises of the semi-transparent canopy through which the sun radiation passes, and the ground material, which functions as a heat exchanger that transfers the gained thermal energy to the adjacent air for the system operation. The ground absorber is also a heat storage medium where some of the energy gained from the sun in the form of heat is transferred by conduction through the layers of the ground and stored for future use when there is absence of solar radiation or on cloudy days. Some losses occur at the collector through the transparent cover and to the earth core which is reported to be about 50% [17].

The mathematical analysis of the collector for the proposed model is developed with the assumptions that the flow through the system is steady and that the flow from the collector periphery towards its center is one-dimensional. The temperature of the air at the collector inlet is assumed to be equal to the ambient temperature. The total energy available to a SCPP collector, Q_{solar} is shown in Equation 1, where I is the solar irradiance (W/m^2) and A_{solar} is the surface area of the collector (m^2).

$$Q_{solar} = I \cdot A_{col} \tag{1}$$

The energy absorbed and utilized by the collector, Q_{col} (W), is shown in Equation 2, where it is the sum of heat absorbed by the collector from the ground and from the canopy cover, Q_{ground} and Q_{canopy}, respectively.

$$Q_{col} = Q_{ground} + Q_{canopy} \tag{2}$$

The absorbed energy by the ground is given by Equation 3 and the absorbed energy of the collector roof is given by Equation 4.

$$Q_{ground} = Q_{solar} \cdot \alpha_{ground} \cdot \tau_{canopy} \tag{3}$$

$$Q_{canopy} = Q_{solar} \cdot \alpha_{canopy} \tag{4}$$

From the above equations, α_{canopy} and α_{ground} are the absorptivity property of the canopy and the ground, and τ_{canopy} is the transmissivity of the transparent canopy cover.

2.2 The Solar Chimney

The mass flow rate of air that passes through the solar chimney component depends largely on the pressure difference between the buoyant air at the chimney base and the ambient pressure at the chimney exit (ΔP_{total}). The total pressure difference created in the chimney after excluding losses due to friction can be expressed as:

$$\Delta P_{total} = \int_0^H g\left(\rho_{exit} - \rho_{base}\right) dy \tag{5}$$

After considering dry air inside the chimney, the air density can be expressed as:

$$\rho_{air} = \rho_{amb}\left[1-\beta\left(T_{air}-T_{amb}\right)\right] = \rho_{amb} - \rho_{amb}\left(\frac{T_{air}-T_{amb}}{T_{amb}}\right) \quad (6)$$

where the β is the coefficient of thermal expansion, expressed as the inverse of ambient temperature.

After substituting Equation 6 into Equation 5, ΔP_{total} can be written as:

$$\Delta P_{total} = \int_0^H \rho_{amb} g\left(\frac{T_{air}-T_{amb}}{T_{amb}}\right)dy \quad (7)$$

Then ΔP_{total} will be:

$$\Delta P_{total} = \rho_{amb} gH\left(\frac{T_{air}-T_{amb}}{T_{amb}}\right) \quad (8)$$

where *H* is the height of the chimney.

2.3 Conservation of Mass, Momentum, and Energy

For the two-dimensional, steady-state model, the continuity equation is given by Equation 9.

$$\frac{\partial(\rho u)}{\partial z} + \frac{1}{r}\frac{\partial(r\rho v)}{\partial r} = 0 \quad (9)$$

The momentum equations are given by Equations 10 and 11, and the energy equation is given by Equation 12 [18], [19]. The incompressible flow assumption is valid as the maximum Mach number does not reach the value of 0.1. To manipulate the effects of buoyancy in the air, the Boussinesq hypothesis is utilized, which defines the thermal expansion coefficient, β in Equation 13 [20].

$$\frac{\partial(\rho uu)}{\partial z} + \frac{1}{r}\frac{\partial(r\rho uv)}{\partial r} = \frac{\partial p}{\partial z} + (\rho-\rho_0)g + 2\frac{\partial}{\partial z}\left[(\mu+\mu_t)\frac{\partial u}{\partial z}\right] + \frac{1}{r}\frac{\partial}{\partial r}\left[(\mu+\mu_t)r\left(\frac{\partial u}{\partial z}+\frac{\partial v}{\partial r}\right)\right] \quad (10)$$

$$\frac{\partial(\rho uv)}{\partial z} + \frac{1}{r}\frac{\partial(r\rho vv)}{\partial r} = -\frac{\partial p}{\partial r} + \frac{\partial}{\partial z}\left[(\mu+\mu_t)\left(\frac{\partial v}{\partial z}+\frac{\partial u}{\partial r}\right)\right] + 2\frac{1}{r}\frac{\partial}{\partial r}\left[(\mu+\mu_t)r\left(\frac{\partial v}{\partial r}\right)\right] - \frac{2(\mu+\mu_t)v}{r^2} \quad (11)$$

$$\frac{\partial uT}{\partial z} + \frac{1}{r}\frac{\partial(rvT)}{\partial r} = -\frac{1}{\rho} + \frac{\partial}{\partial z}\left[\left(\frac{\mu}{Pr}+\frac{\mu_t}{\sigma_t}\right)\frac{\partial T}{\partial z}\right] + \frac{1}{\rho r}\frac{\partial}{\partial r}\left[\left(\frac{\mu}{Pr}+\frac{\mu_t}{\sigma_t}\right)r\frac{\partial T}{\partial z}\right] \quad (12)$$

$$\beta = -\frac{1}{\rho}\left(\frac{\partial\rho}{\partial T}\right)_P \approx -\frac{1}{\rho}\left(\frac{\rho_0-\rho}{T_0-T}\right) \quad (13)$$

Assuming small temperature variations in the chimney system, the density could be expressed as [20]:

$$(\rho_0-\rho) \approx -\rho_0\beta(T_0-T) \quad (14)$$

where "0" in the subscript indicates a reference value, and the density could be predicted based on this preset reference parameter. The reference density is a constant and is substituted into the mass and energy equations. For the buoyancy term in the momentum equation, this approximation considers the density as a function of temperature, and the flow is driven by the gravity force [20].

2.4 Radiation Model

The Discrete Ordinates (DO) model available in ANSYS is used to solve the radiation heat transfer in the system using the surface-to-surface radiation heat transfer through semi-transparent materials.

In this study, the canopy material is specified as Perspex, assuming that it has the same behavior for all radiation wavelengths. The DO model works well throughout an entire range of optical thicknesses and could be used to compute non-gray radiation by utilizing a gray band model.

2.5 Performance Indicator and Collector Efficiency

The performance indicator (P.I.) for the proposed model is calculated as a product of the increase in air temperature inside the system, ΔT, and the air mass flow rate through the chimney, $\dot{m}$ [21].

$$P.I. = \dot{m}\cdot\Delta T \quad (15)$$

$$\Delta T = T_{air} - T_{amb} \quad (16)$$

$$\dot{m} = \rho A_{ch} V_{ch} \quad (17)$$

The efficiency of the collector, η_{col}, is a ratio of the thermal energy gained by the air inside the system to the input energy into the system from the sun, Q_{solar} [21].

$$\eta_{col} = \frac{\dot{m} c_p \Delta T}{Q_{solar}} \quad (18)$$

3. EXPERIMENTAL IMPLEMENTATION

A solar chimney power plant model was fabricated and tested under real conditions in the Solar Research site at Universiti Teknologi PETRONAS, Seri Iskandar, Perak, Malaysia (Latitude: 4° 23' 17.68" N and Longitude: 100° 58' 28.61" E). The experimental investigation included two main cases: a bare chimney and a chimney with a heat trap. Each case was tested with three different collector sizes, creating 6 cases. The following subsections describe the methodology in detail.

3.1 Model Description and Experimental Setup

The solar chimney experimental model was built with a transparent collector canopy, a chimney, and a ground thermal absorbing medium. The canopy is made of 4-mm-thick Perspex glass, with transmission coefficient of 0.92 [22], supported by iron frames. The canopy frames for the full setup were constructed with two angles of inclination, as indicated in Figure 2. The inner section of the canopy of 2.4 m diameter was connected from the chimney base, sloped at 20° from the horizontal, and ended approximately 0.4 m off the ground, as shown in Figure 3. The outer canopy was connected to the inner canopy, at a slope of 5° from the horizontal, and extended out to 4.16 m diameter. Further extension to the collector was made permitting the total diameter of the collector for the full setup to be 6.6 m. The canopy inclination angles were selected as such for combined reasons. The low angle of 5° from the horizontal allows effective heat transfer to the air between the surfaces in the outer section of the collector. Increasing the angle to 20° from the horizontal in the inner section of the canopy avoids the abruptness or air convergence and reversal of the air stream towards the chimney [23].

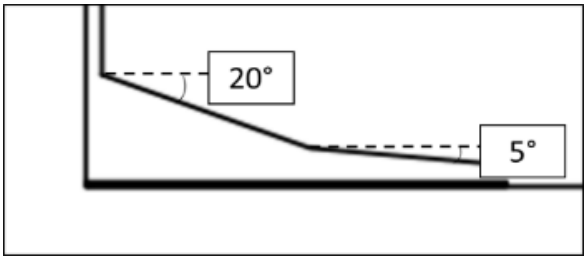

Fig. 2. Double inclination angle of the canopy.

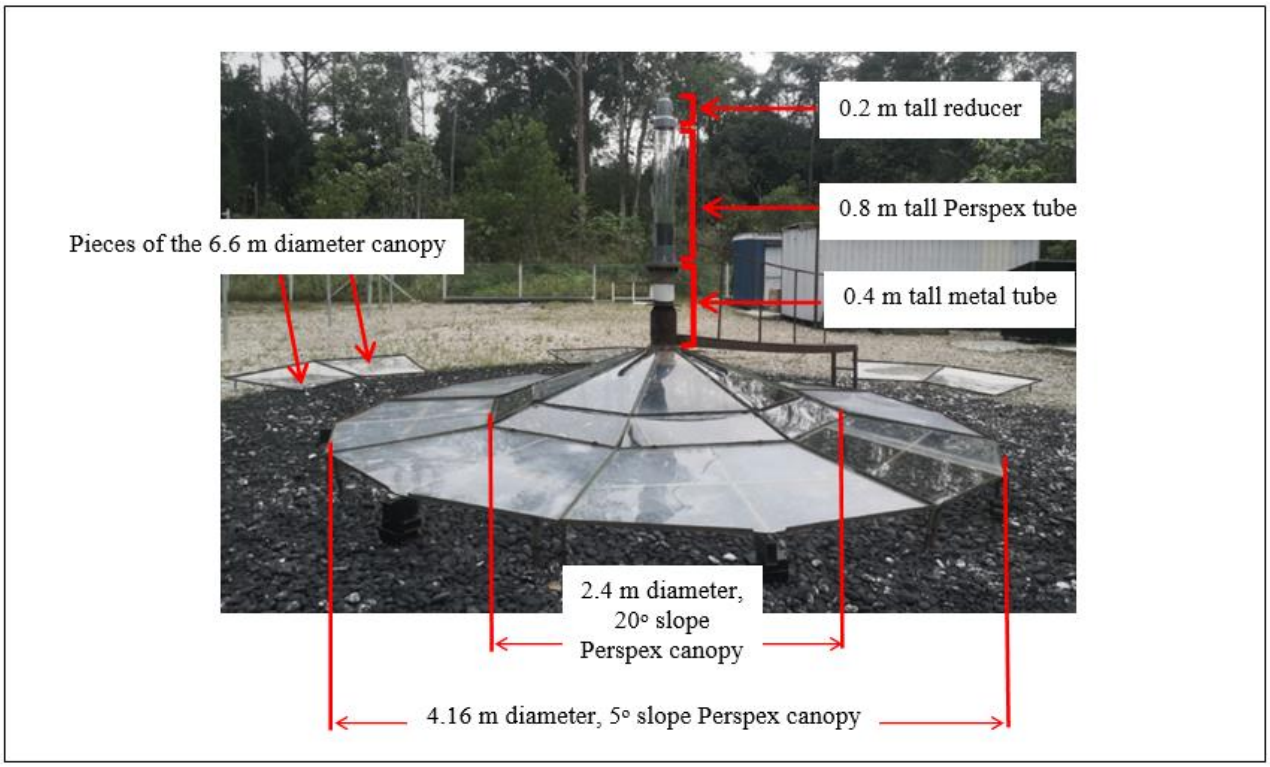

Fig. 3. Experimental setup with a mock chimney, 4.16 m canopy diameter.

Details in Figure 3 show the cases of 2.4 m and 4.16 m diameters. The extension pieces of the canopy for the full 6.6 m diameter setup were laid outside the experimental rig and could be connected to the 4.16 m frames. The ground surface component under the collector comprised of pebbles that were painted black

with approximately 100 mm thickness, acting as thermal absorption medium. This gave the ground an emissivity of 0.95 [24]. Furthermore, it was the least costly material compared to others with similar solar radiation coefficients [25], [26]. This setup was used throughout the investigation presented in this paper.

A mock chimney was used in the setup of the investigation presented here, as shown in Figure 3. It was made of a 0.8-m-tall Perspex tube with a 0.2 m PVC reducer fixed at the top end. The Perspex is selected to allow solar penetration, and the reducer will create a high velocity at the top (chimney outlet) that is typically obtained from a tall chimney. The Perspex tube is connected to the lower metal part of the chimney by a flange. The dimension of the plant is summarized in Table 1. In the conventional design of the solar chimney research model, the chimney is made of a 14-m-tall PVC tube located at the center of the collector. In this taller chimney where a reducer is not required, the Perspex tube would still be attached to the top of the chimney as part of the heat trap assembly described below.

To create the heat trap, an aluminium plate was coated with a mixture of matte black paint and aluminium oxide. Then the plate was inserted along the inside wall of the Perspex chimney tube, creating a circular cross-section, as shown in Figure 4.

In big-scale applications where the chimney diameter is large, the transparent tube is not necessary as the size of the chimney allows solar radiation penetration onto the heat absorber plate.

Table 1. Dimensions of the experimental setup.

Parameter	Dimension
Collector diameter	2.40 m, 4.16 m, 6.60 m
Collector height at peripheral inlet	0.10 m to 0.40 m
Canopy inclination	Inner section 20°, outer section 5°
Perspex chimney height (without reducer)	0.80 m
Total chimney height	1.20 m
Chimney diameter	0.152 m

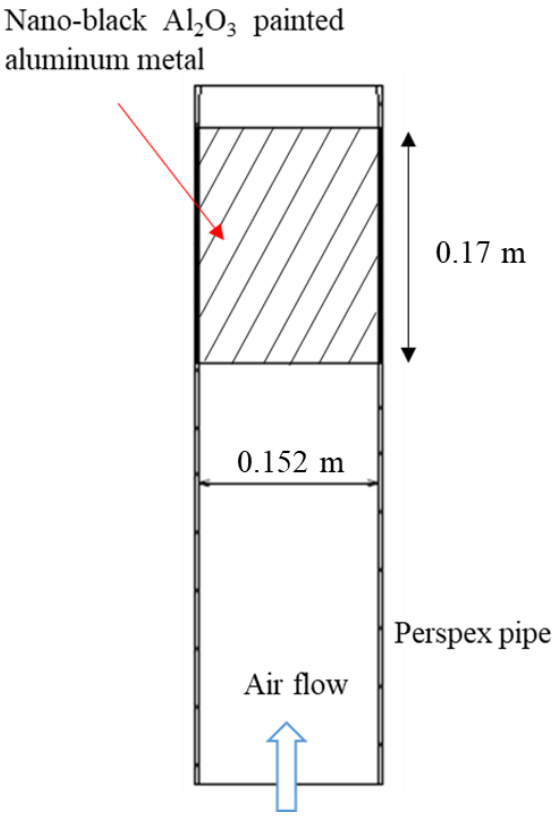

Fig. 4. Specification of the heat trap assembly.

3.2 Measuring Instruments and Uncertainties

Temperature readings were taken at different locations using Type K surface thermocouples, which were connected to the GRAFTECH midi GL820 digital data logger. Airflow velocity data were read using the hotwire-probe and vane-probe sensors connected to the

digital anemometer model TPI 575C1. The total solar intensity was measured using a digital solarimeter that was fixed at ambient.

Confidence in the measurement of the variables could be identified by the accuracy level of the measuring devices. Table 2 presents the used instruments and the specifications of each device, including the provided accuracy by the supplier.

3.3 Data Acquisition

For each case, measurements were taken between 12:00 pm to 3:00 pm at an hourly interval. The reason for recording the data between these hours was that the impact of solar irradiance on the system performance will be highest when solar irradiance is high (600 W/m^2 to 1000 W/m^2). Hence any difference between the cases would be most apparent during these hours.

The bare chimney cases were first investigated for collector diameters 2.40 m (case 1-a), 4.16 m (case 1-b), and 6.60 m (case 1-c). The heat trap was then installed, and the measurements were repeated for collector diameters 2.40 m (case 2-a), 4.16 m (case 2-b), and 6.60 m (case 2-c).

Table 2. Details and accuracy of the measuring instruments.

Parameter	Instrument	Range	Reading Accuracy
Solar radiation	KIMO-SL 200 solarimeter	1 to 1300 W/m^2	±5%
Surface temperature	- GRAPHTEC GL820 data logger	–200 to 1260°C	±0.05%
	- Type-K thermocouple wire		±0.75%
Air temperature	- GRAPHTEC GL820 data logger	–200 to 1260°C	±0.05%
	- Temperature probe		±0.75%
Air velocity	TPI 575C1 digital reader with hot wire velocity probe	Vane:	±2%
		0.4 to 25m/s	±5%
		Hot wire:	
		0.2 to 20 m/s	

4. NUMERICAL SIMULATION

This section describes the CFD method applied to study the fluid flow and thermal processes within the computational domain of the solar chimney. The commercial package ANSYS Fluent 18 was utilized to model and run the simulations.

4.1 Computational Modeling and Meshing

A 2-D model was created using SpaceClaim software based on the actual geometries of the experimental model described in Section 3.1. The material specifications of the plant are defined in Table 3 [27]. A mesh independence study was conducted, and the details of each mesh model and the accuracy of results are summarized in Table 4. Based on the mesh dependence checking criteria, mesh model 3 was selected for further analysis with 17929 elements.

4.2 Boundary Conditions

For the solar chimney simulation model, boundary conditions were prescribed for each component, as shown in Figure 5. The material selected for the ground, canopy, chimney wall, and heat trap were set according to experimental parameters. The boundary conditions for the computation domain's inlet and outlet were set with zero-gauge pressure. In solar chimney simulations modelled in 2-D, incident solar radiation through the semi-transparent canopy to the ground is commonly set as heat flux or an internal heat source. Temperatures were set based on experimental measurements.

Table 3. Material specifications used in the investigation are based on the experimental setup. [27]

Physical property	Canopy	Ground	Chimney (tall)	Heat Trap
Material	Perspex	Black pebble	PVC	Black painted aluminium
Absorption coefficient	0.06	0.9	0.04	0.9
Transmission coefficient	0.92	0	0	0.05
Density (kg/m^3)	2700	2640	833	2719
Specific heat (J/kg·K)	840	820	1170	871
Thermal conductivity (W/m·K)	0.78	1.73	0.19	260.4
Emissivity	0.9	0.9	0.91	0.7

Table 4. Different models tested for the grid independence study.

Mesh model	Element count	Mass flow rate (kg/s)	% Diff.	Velocity (m/s)	% Diff.
1	4364	0.097777	4.40%	0.511	22.1%

2	7880	0.093477	1.23%	0.398	18.8%
3	17929	0.092331	0.42%	0.323	4.95%
4	27345	0.091946	-	0.307	-

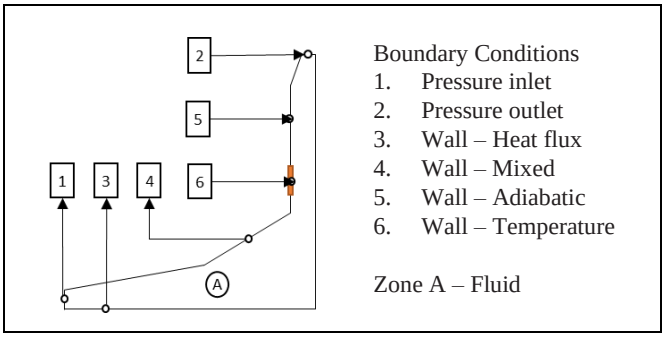

Fig. 5. Boundary conditions for the simulation.

5. EXPERIMENTAL RESULTS

The experiment was conducted over two different days: day 1 for cases 1–a, 1–b, and 1–c, and day 2 for cases 2–a, 2–b, and 2–c. The solar irradiance and ambient temperature measurements for these two days are shown in Figure 6. While at 12:00 pm, the solar irradiance between days 1 and 2 was similar. However, for day 1, during which the bare chimney measurements were taken, solar irradiance was higher by an average of 14% from 1:00 pm to 3:00 pm. Comparison of the ambient air temperature readings between the two days shows that ambient air temperature increased at the same rate as solar irradiance, which supports that all the temperature readings can be taken based on solar irradiance variation.

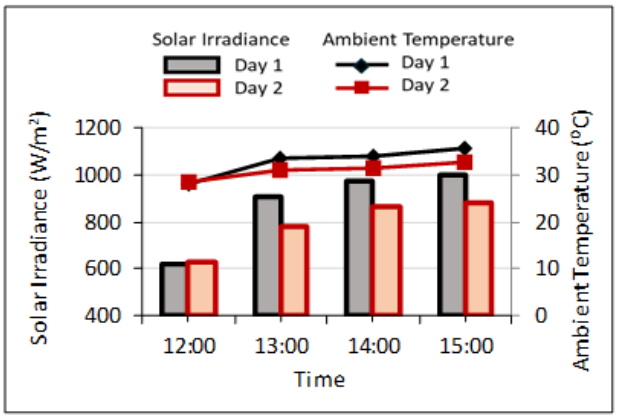

Fig. 6. Solar irradiance for days 1 and 2, recorded between 12:00 pm and 3:00 pm.

5.1 Average Temperature Rise in the Chimney

To evaluate the effectiveness of the heat trap, the temperature readings of air at the chimney outlet are one of the most direct measures when compared with the ambient temperature for each case. This parameter is called the temperature rise. When the solar irradiance was 620 - 630 W/m^2, the average temperature rise was 3.57 $^{\circ}$C. In comparison with the model with heat trap, the average temperature rise was 4.23 $^{\circ}$C. This translated to an improvement of 18.5% in temperature rise for the model with heat trap at lower solar irradiance. At higher solar irradiance of 878 – 910 W/m^2, the temperature rise for the bare model was 3.97 $^{\circ}$C, and for the model with heat trap is 7.27 $^{\circ}$C, which is an improvement of 83.1% at higher solar irradiance. Figure 7 illustrates that the average temperature rise in the model with heat trap increased with increasing solar irradiance more than in the bare model. This shows that the heat trap is more effective with higher solar irradiance at increasing the temperature in the chimney. The heat storage capacity of the heat trap may explain this; as the day progresses and solar irradiance increases, the heat trap can store more energy and transfer it as heat to the air in the chimney.

5.2 Average Air Velocity at Chimney Outlet

At lower solar irradiance of 620 - 630 W/m^2, the air velocity at the chimney outlet was close in both cases, at approximately 0.20 m/s. As solar irradiance increased to 878 – 910 W/m^2, the average outlet air velocity in the bare model was 0.47 m/s, and in the model with heat trap was 0.77 m/s. Figure 8 shows the average air velocity trend recorded at the chimney outlet. In both cases, air velocity increased with solar irradiance. At all levels of solar irradiance, the average air velocity for the heat trap cases surpassed those of the bare chimneys.

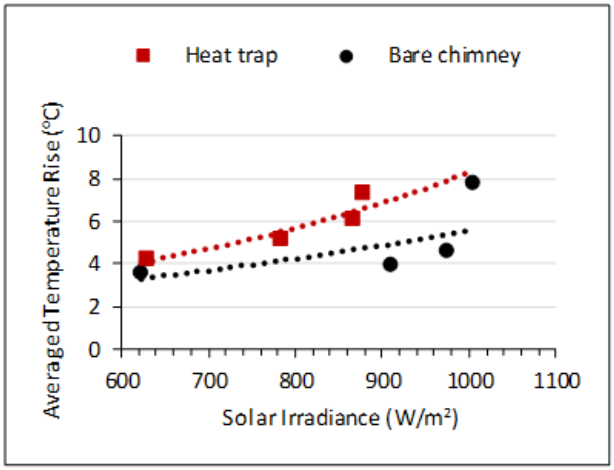

Fig. 7. Average temperature rise achieved between the bare chimney and heat trap cases.

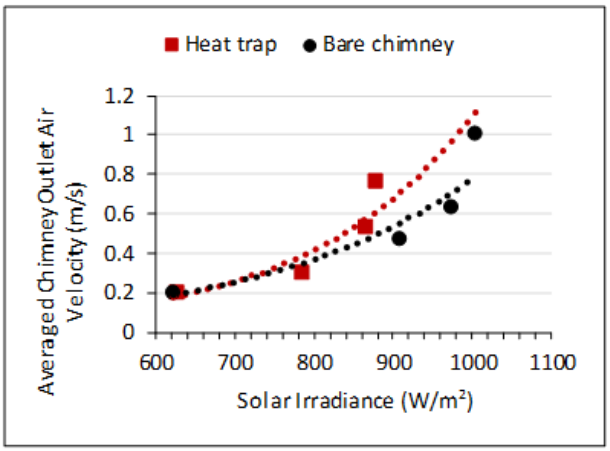

Fig. 8. Average velocity of air at the chimney outlet between bare chimney and heat trap cases.

5.3 *Effect of Collector Size*

The effect of changing the collector size on the solar chimney performance can be seen in Figures 9 (a) and (b). The performance indicator (P.I.) is calculated using Equation 15.

All cases were analyzed at two levels of solar irradiance: 650 W/m^2 and 850 W/m^2. For the bare chimney at 650 W/m^2, the P.I. for cases 1–a and 1–b were 0.01655 and 0.01651 kg·K/s, respectively, which is a 0.24% difference. In case 1–c, the P.I. increased to 0.02265 kg·K/s, which is 37.2% higher than in case 1–b. At 850 W/m^2, the P.I. for the three cases were 0.03539, 0.04579, and 0.05915 kg·K/s, respectively, which is equivalent to 29.0% improvement in the P.I. when comparing cases 1–a and 1–b, and between cases 1–b and 1–c.

For the models with heat trap at 650 W/m^2, the P.I. for cases 2–a, 2–b, and 2–c were 0.004146, 0.01186, and 0.0202 kg·K/s, respectively, which is an improvement of 186% and 70.3% each as the collector diameter was increased. These results indicate that the increase in collector size, combined with the heat trap assembly, may significantly improve the SC performance in terms of temperature rise and mass flow rate even at lower solar irradiance.

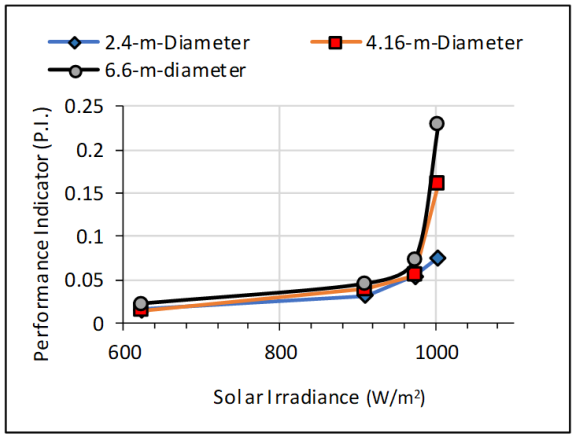

(a)

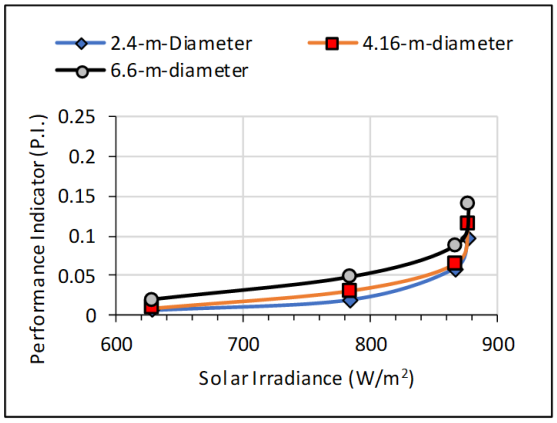

(b)

Fig. 9. Performance indicators (P.I.) for different collector sizes for the (a) bare chimney and (b) heat trap cases.

5.4 *Averaged Performance Indicator and Collector Efficiency*

The system's performance with and without a heat trap was averaged for all the collector diameter cases and presented in Figure 10. The trend indicates that the P.I. improved with the heat trap as solar irradiance increased. The P.I. was predicted and compared for two solar irradiance levels in Table 5.

Table 5. Predicted P.I. comparison of the SC with and without heat trap assembly.

Solar irradiance (W/m^2)	P.I. Bare chimney (kg·K/s)	P.I. Heat trap (kg·K/s)	Percentage increase (%)
750	0.0281	0.0327	16.05
950	0.0639	0.1752	174.23

From 750 W/m^2, the P.I. for the bare chimney and heat trap cases were 0.0281 and 0.0327 kg·K/s, respectively, which is a 16.4% improvement in the model with heat trap assembly. At 950 W/m^2, the P.I. values increased to 0.0639 and 0.1752 kg·K/s, which is a 174.2% increase in the model with the heat trap assembly. This finding indicated that as solar irradiance increased through the day, the heat trap was effective as a heat storage medium and at transferring the heat to the air in the chimney.

The collector thermal efficiency was calculated using Equation 18 and presented in Figure 11. For the 2.4-m-diameter collector, the model with heat trap showed higher collector efficiency at 1.25%, compared to the bare model at 0.96%. The trend continued for the models with 4.16-m-diameter and 6.6-m-diameter, which showed that the heat trap model recorded a higher collector efficiency than the bare model. For this investigation, the collector efficiency must not be analyzed by different collector sizes but by the heat trap addition at a specific collector size. This is because the

collector efficiency is proportional to the mass flow rate of air through the system. The constant chimney height throughout the investigation maintained the stack effect that drives the flow through the system. At the same time, the energy input into the system increases with increasing collector canopy area. This directly reduces the thermal efficiency of the larger collectors in this investigation. However, at specific collector sizes, the effect of the heat trap assembly was significant and positive compared to the bare chimney model.

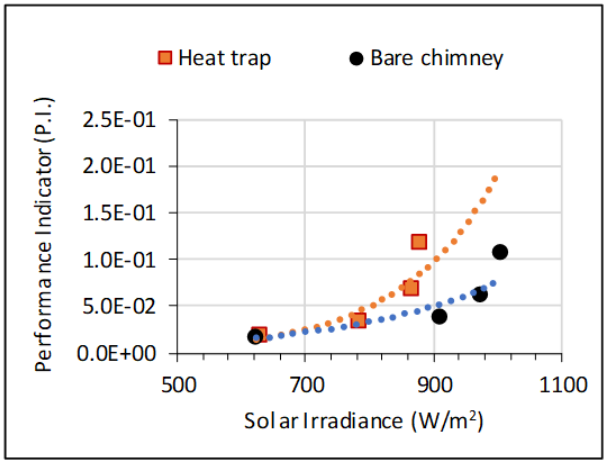

Fig. 10. The system's average performance between bare chimneys and heat trap cases.

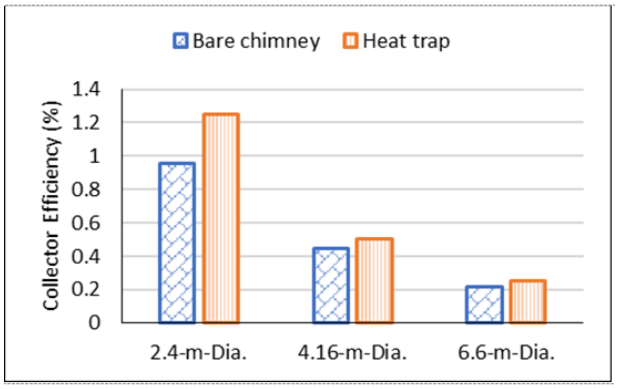

Fig. 11. Collector efficiency between bare chimney and heat trap cases at all collector sizes.

6. SIMULATION RESULTS

The results from the simulation provided more insight into the velocity and temperature trends in the chimney, both with and without a heat trap. Validation of the simulation procedure was conducted by comparing the results with experimental data presented in the previous section. Two cases were investigated with a 6.60-m collector diameter based on models 1–c (bare chimney) and 2–c (with heat trap).

6.1 Validation of Numerical Results

The bare case (based on model 1–c) was checked against experimental data of the same design for validation. The air outlet temperature values for the experiment and simulation were 317.0 K and 311.7 K, respectively, which is a difference of 1.7%. The air outlet velocity for the experiment and simulation were 0.8 m/s and 0.812 m/s, respectively, which is a difference of 1.5%. The computational simulation was performed using constant ambient conditions as recorded in the relevant experiment with solar irradiance of 1000 W/m^2. This simplification would not impact the main objective of this paper in a significant way since it is a comparison between various design conditions under the same weather conditions.

The computational simulation procedure is acceptable as the percentage of the difference between the experiment and simulation data is within a reasonable agreement.

6.2 Chimney with Reducer – Temperature Results

To quantify the trap's effectiveness in transferring heat to the airflow, Figure 12 compares the airflow temperature at the top of the chimney along its diameter. The higher temperature in the fluid zone at the heat trap region was apparent near the chimney walls. For the bare chimney model, the temperature at the flow center was 321.45 K, which reduced to 321.08 K at the chimney wall. With the heat trap, the air temperature at the flow center was 321.45 K and it increased to 326.76 K near the wall (heat trap surface). There was a 12.75% increase in average temperature rise across the chimney diameter at the heat trap region.

6.3 Chimney with Reducer – Velocity Results

Due to the generally low air velocity in these investigations, the effect of the heat trap could be seen clearly in the contours of velocity magnitudes, as shown in Figures 13 (a) and (b). In Figure 13 (a), air velocity was highest at the center and reduced gradually towards the chimney wall. For the model with heat trap in Figure 13 (b), there was an increase in air velocity away from the wall that was higher than the velocity at the center. This finding coincided with the plot of air temperature in Figure 12, where the increase in air temperature near the heat trap surface lowered the air density in that region slightly and enhanced its buoyancy, therefore driving more air out of the outlet. By design, the reducer's effect in increasing the flow's velocity was apparent as the air velocity increased rapidly at the top of the reducer at the outlet. In fact, the higher velocity caused by the reducer was greater than the heat trap's effect in increasing air buoyancy in these investigations.

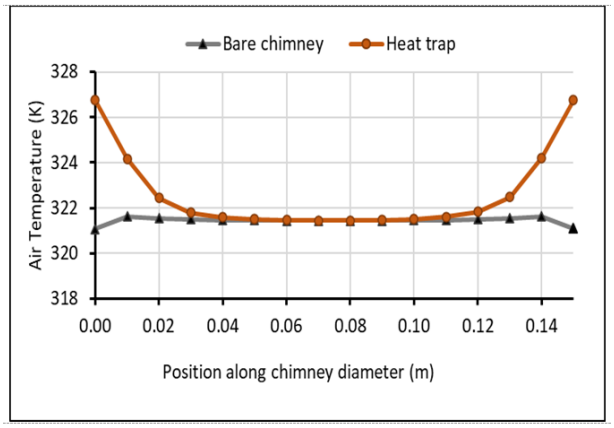

Fig. 12. Air temperature profile before the chimney outlet, plotted along the chimney diameter.

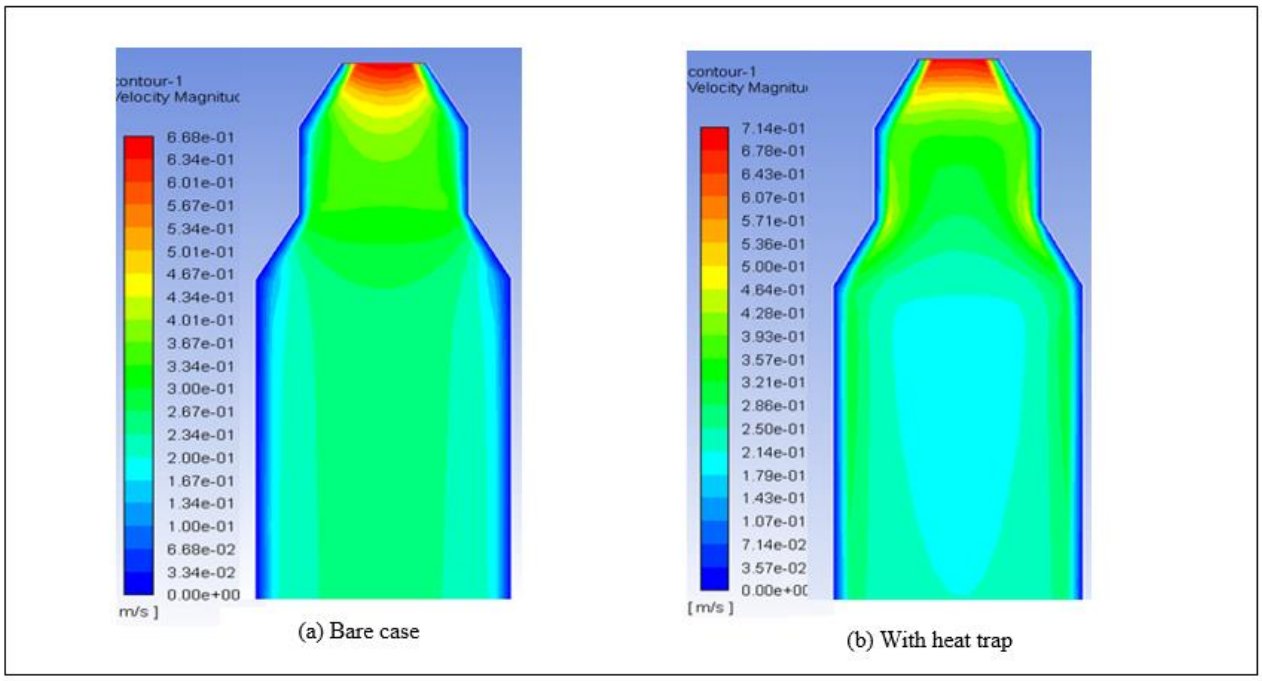

Fig. 13. Contours of the air velocity magnitude at the chimney top for 6.6-m collector diameter.

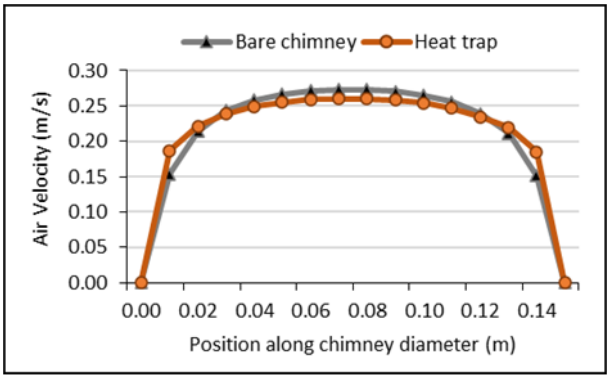

Fig. 14. Air velocity profile at the chimney top (before reducer section).

Figure 14 compares the air velocity plot at the top of the chimney along the chimney diameter. or the bare chimney model, air velocity at the flow center was maximum at 0.273 m/s and reduced to zero at the chimney wall. With the heat trap, the air velocity at the flow center was maximum at 0.260 m/s. While this value is lower compared to the bare case, the heat trap improves the buoyancy of air near its surface, increasing the velocity of air near the walls.

6.4 Simulation with 14-m Chimney

A numerical simulation was done for an SC model with a 14-m chimney. The modelling approach is identical to that described in sections 4.1 and 4.2 for all the design parameters; the difference in this model is that the 14-m chimney made of PVC replaces the mock chimney with the reducer described in the previous simulation model. The collector diameter was maintained at 6.60 m for all simulations.

The motivation for investigating this model was to gain insight into the velocity trends at the top of the chimney with and without the heat trap assembly. As seen in previous simulation results for velocity (Figure 13), the effect of the reducer in increasing the air velocity at the outlet was greater than the enhanced air buoyancy from the temperature rises due to the heat trap. The model presented in this section may provide more insight as its design is closer to the real solar chimney model with typically tall chimneys. The numerical simulation was performed on three models: (1) a bare chimney (PVC), (2) a bare chimney (PVC) extended with heat trap assembly, and (3) a bare chimney (PVC) with a similar height to model (2). The heat trap assembly that is added to model (2) is based on the experimental model of the heat trap, which is made of a Perspex tube and inserted with a nano-painted aluminium metal, as shown in Figure 4.

The bare chimney model showed a constant temperature profile across the diameter, at 316.8 K, while the heat trap model shows that the temperature increased to 317.6 K near the wall. This shows convection heat transfer between the heat trap and the air inside the chimney. However, this energy transfer is limited to the air in the near-wall regions due to the moving air flow toward the chimney outlet.

Figure 15 shows the temperature contour of air at the top region of the chimney with a heat trap. At the heat trap surfaces, air temperature was up to 330 K. There was a 4.31% increase in average temperature rise across the chimney diameter at the heat trap region.

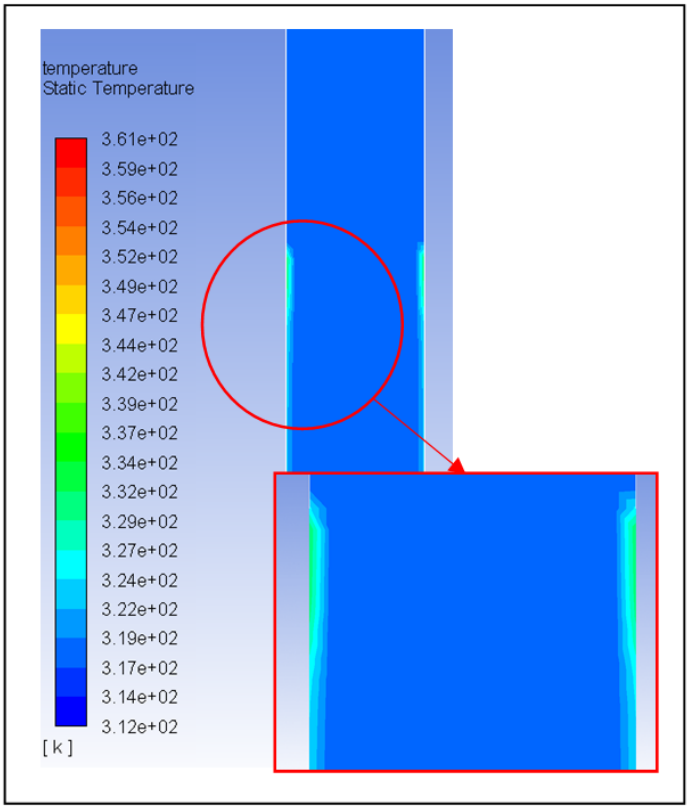

Fig. 15. Air temperature contours at the chimney outlet region for the 15-m chimney with heat trap.

The centerline air velocity for the bare chimney and heat trap cases were 0.150 m/s and 0.157 m/s, respectively. The velocity was higher in the heat trap model as the flow approached the heat trap surface. This tied in with the increase in air temperature calculated at this region, which translated to lower density and higher mobility of air in the region near the walls.

The mass flow rate results for Model (1) recorded a value of 0.2615 kg/s. When the heat trap assembly was added at the chimney exit in the model (2), the mass flow rate is 0.2630 kg/s, which is a 0.57% improvement. For model (3) with the 15-m chimney and no heat trap, the mass flow rate is 0.2623 kg/s. The increase in performance indicator is 5.5% when the heat trap assembly is added at the top of the chimney. Compared with simply adding an equivalent height of the same chimney material, which gives a 0.8% improvement, the heat trap drives the flow out of the system more.

7. CONCLUSIONS

Experimental and numerical investigations were conducted to test the performance of a heat trap assembly made of a nano-painted aluminum plate, improving the flow inside the chimney of a solar chimney power plant. From the experimental and numerical results, the following conclusions can be made:

- The heat trap could store energy and enhance the heat transfer to the air in the chimney later in the day, regardless of the collector's size.
- An increase of 83.1% in air temperature at the top of the chimney model was seen with the proposed heat trap assembly. The performance indicator, P.I., showed an improvement of up to 174.2% at higher solar irradiance levels.
- From the simulation, temperature results showed that air temperature started to increase near the walls from the heat trap location. An increase of 4.31% in average temperature rise was seen at the chimney outlet with the 14-m chimney with heat trap.
- The performance indicator, P.I., showed an improvement of 5.5% when a heat trap was modelled on the 14-m chimney, which was more than the improvement shown by simply extending the height of the bare chimney.

The effectiveness of the heat trap in the experimental setup with mock chimney and the numerical simulation encourages the construction of the heat trap on a real 14-m tall chimney, and pilot plants of bigger scales. Its performance could be analyzed further to test the effects with real environmental conditions including ambient winds. The heat trap's ability to increase the plant performance may eliminate the need for increasing chimney height, which may reduce construction cost and complexity.

REFERENCES

[1] Weli R.B., Atrooshi S.A. and Schwarze R., 2021. Investigation of the performance parameters of a sloped collector solar chimney model – An adaptation for the North of Iraq. *Renewable Energy* 176: 504–519. https://doi.org/10.1016/j.renene.2021.05.075.

[2] AL-Bonsrulah H.A.Z., Danook S.H., Alshukri M.J., Ahmed A.M., Raja V., Veeman D., Al-

Bahrani M., 2023. CFD modeling of a horizontal wind turbine by utilizing solar nozzle for power production. *International Journal of Low-Carbon Technologies* 18: 31-37, https://doi.org/10.1093/ijlct/ctac127.

[3] Harte R., Graffmann M. and Krätzig W.B., 2013. Optimization of solar updraft chimneys by nonlinear response analysis. *Applied Mechanics and Materials* 283: 25–34. https://www.scientific.net/AMM.283.25.

[4] Yapıcı E.Ö., Ayli E. and Nsaif O. 2020. Numerical investigation on the performance of a small scale solar chimney power plant for different geometrical parameters. *Journal of Cleaner Production* 276. http://dx.doi.org/10.1016/j.jclepro.2020.122908.

[5] Mullett L.B. 1987. The solar chimney-overall efficiency, design and performance. *International Journal of Ambient Energy* 8(1): 35-40. https://doi.org/10.1080/01430750.1987.9675512

[6] Ganguli A.A. and S. Deshpande, 2020. Three dimensional CFD studies of a solar chimney: effect of geometrical parameters and diurnal variations on power generated. *Frontiers in Chemical Engineering* 2. https://doi.org/10.3389/fceng.2020.00002.

[7] Bergermann R. and J. Schlaich. 2010. Concept and motivation of solar updraft power technology. In Proceedings of the 2nd International Conference on Solar Chimnet Power Technology, Bochum, Germany, 28-30 September 2010.

[8] Cottam P.J., Duffour P., Lindstrand P. and Fromme P., 2019. Solar chimney power plants – Dimension matching for optimum performance. *Energy Conversion Management* 194: 112–123. https://doi.org/10.1016/j.enconman.2019.04.074.

[9] Guo P., Li J., Wang Y. and Wang Y. 2015. Numerical study on the performance of a solar chimney power plant. *Energy Conversion and Management* 105: 197–205.http://dx.doi.org/10.1016/j.enconman.2015.07.072.

[10] Mehranfar S., Gharehghani A., Azizi A., Mahmoudzadeh Andwari A., Pesyridis A. and Jouhara H., 2022. Comparative assessment of innovative methods to improve solar chimney power plant efficiency. *Sustainable Energy Technology Assessments* 49: 101807. https://doi.org/10.1016/j.seta.2021.101807.

[11] Khidhir D.K. and S.A. Atrooshi. 2019. Investigation of thermal concentration effect in a modified solar chimney. *Solar Energy* 206: 799–815.https://doi.org/10.1016/j.renene.2021.05.075

[12] Kebabsa H., Said Lounici M., and Daimallah A. 2021. Numerical investigation of a novel tower solar chimney concept. *Energy* 214: 119048. https://doi.org/10.1016/j.energy.2020.119048.

[13] Saleh M.J., Atallah F.S., Algburi S., and Ahmed O.K., 2023. Enhancement methods of the performance of a solar chimney power plant: Review. *Results in Engineering* 19: 101375. https://doi.org/10.1016/j.rineng.2023.101375.

[14] Rahimi Larki M., Hosseini R., Rahimzadeh H., and Sarlak H., 2021. Performance analysis of a laboratory-scale tilted solar chimney system exposed to ambient crosswind. *Renewable Energy* 164: 1156–1170. https://api.semanticscholar.org/CorpusID:228849798.

[15] Pradhan S., Chakraborty R., Mandal D.K., Barman A., and Bose P., 2021. Design and performance analysis of solar chimney power plant (SCPP): A review. *Sustainable Energy Technology Assessments* 47 (February): 101411. https://doi.org/10.1016/j.seta.2021.101411.

[16] Zhou X., Yang J., Xiao B., and Hou G. 2007. Experimental study of temperature field in a solar chimney power setup. *Applied Thermal Engineering* 27(11–12): 2044–2050. http://dx.doi.org/10.1016/j.applthermaleng.2006.12.007.

[17] dos S. Bernardes M.A., Voß, A., and Weinrebe G. 2003. Thermal and technical analyses of solar chimneys. *Solar Energy* 75(6): 511–524. https://doi.org/10.1016/j.solener.2003.09.012.

[18] Ayadi A., Bouabidi A., Driss Z., and Abid M.S., 2018. Experimental and numerical analysis of the collector roof height effect on the solar chimney performance. *Renewable Energy* 115: 649–662. https://doi.org/10.1016/j.enbuild.2017.01.047.

[19] Ayadi A., Nasraoui H., Bouabidi A., Driss Z., Bsisa M., and Abid M.S., 2018. Effect of the turbulence model on the simulation of the air flow in a solar chimney. *International Journal of Thermal Sciences* 130: 423–434. https://doi.org/10.1016/j.ijthermalsci.2018.04.038.

[20] Sangi R., Amidpour M., and Hosseinizadeh B., 2011. Modeling and numerical simulation of solar chimney power plants. *Solar Energy* 85: 829-838. https://api.semanticscholar.org/CorpusID:121100482.

[21] Al-Azawiey S.S., Al-Kayiem H.H., and Hassan S. B., 2016. Investigation on the influnce of collector height on the performance of solar chimney power plant. *ARPN Journal of Engineering and Applied Sciences* 11(20): 12197–12201. https://www.scopus.com/inward/record.uri?eid=2-s2.0-84994242591&partnerID=40&md5=b3bf2c9e42a6233e6e2e813ff7f7aa83.

[22] Aurybi M.A., Al-Kayiem H.H., Gilani S.I.U., and Ismaeel A.A. 2017. Numerical analysis of solar updraft power plant integrated with external heat source. *MATEC Web of Conferences* 131: 01004. http://dx.doi.org/10.1051/matecconf/201713101004.

[23] Cottam P.J., Duffour P., Lindstrand P., and Fromme P., 2016. Effect of canopy profile on solar thermal chimney performance. *Solar Energy* 129: 286–296. https://doi.org/10.1016/j.solener.2016.01.052.

[24] Jamil I.E., Sing C.Y. and Al-Kayiem H.H. 2020. Rudimentary analysis for solar chimney enhancement. *IOP Conference Series Material*

Science and Engineering 863(1): 012063. http://dx.doi.org/10.1088/1757-899X/863/1/012063

[25] Al-Azawiey S.S. and S.B. Hassan. 2016. Heat absorption properties of ground material for solar chimney power plants. *International Journal of Energy Production and Management.* http://dx.doi.org/10.2495/EQ-1-4-403-418.

[26] Buğutekin A., 2012. An experimental investigation of the effect of periphery height and ground. *Journal of Thermal Science and Technology* 32(1): 51–58. https://api.semanticscholar.org/CorpusID:173171921.

[27] Abdul Jamil I.E., Al-Kayiem H.H., Al-Azawiey S.S., and Shyaa A.K., 2024. Critical interpretation and analysis to correlate the canopy height to collector diameter ratio for optimized design of solar chimney power plants. *International Journal of Renewable Energy Devlopment* 13(1): 99–109. https://doi.org/10.14710/ijred.2024.57689.